ACS Catalysis

Research Article

pubs.acs.org/acscatalysis

On the Reaction Mechanism of Acetaldehyde Decomposition on Mo(110)

Donghai Mei,*[,†] Ayman M. Karim,[‡] and Yong Wang[‡,§]

[†]Fundamental and Computational Directorate and [‡]Energy and Environmental Directorate, Pacific Northwest National Laboratory, Richland, Washington 99352, United States

[§]The Gene and Linda Voiland School of Chemical Engineering, Washington State University, Pullman, Washington 99164, United States

ABSTRACT: The strong Mo−O bond strength provides promising reactivity of Mo-based catalysts for the deoxygenation of biomass-derived oxygenates. Combining the novel dimer saddle point searching method with periodic spin-polarized density functional theory calculations, we investigated the reaction pathways of a acetaldehyde decomposition on the clean Mo(110) surface. Two reaction pathways were identified, a selective deoxygenation and a nonselective fragmentation pathways. We found that acetaldehyde preferentially adsorbs at the pseudo 3-fold hollow site in the η^2(C,O) configuration on Mo(110). Among four possible bond (β-C−H, γ-C-H, C−O and C−C) cleavages, the initial decomposition of the adsorbed acetaldehyde produces either ethylidene via the C−O bond scission or acetyl via the β-C−H bond scission while the C−C and the γ-C-H bond cleavages of acetaldehyde leading to the formation of methyl (and formyl) and formylmethyl are unlikely. Further dehydrogenations of ethylidene into either ethylidyne or vinyl are competing and very facile with low activation barriers of 0.24 and 0.31 eV, respectively. Concurrently, the formed acetyl would deoxygenate into ethylidyne via the C−O cleavage rather than breaking the C−C or the C−H bonds. The selective deoxygenation of acetaldehyde forming ethylene is inhibited by the relatively weaker hydrogenation capability of the Mo(110) surface. Instead, the nonselective pathway via vinyl and vinylidene dehydrogenations to ethynyl as the final hydrocarbon fragment is kinetically favorable. On the other hand, the strong interaction between ethylene and the Mo(110) surface also leads to ethylene decomposition instead of desorption into the gas phase.

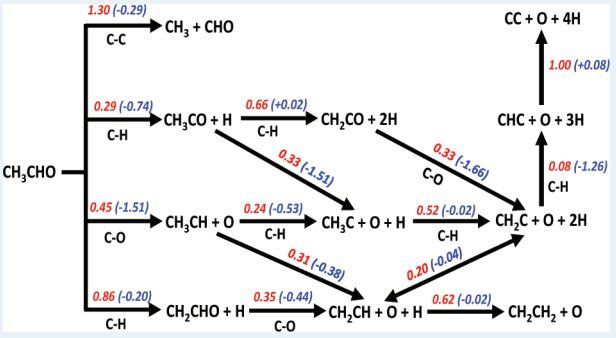

KEYWORDS: *Mo(110), DFT, reaction mechanism, acetaldehyde, deoxygenation*

1. INTRODUCTION

Hydrodeoxygenation (HDO) is one of important catalytic processes for upgrading pyrolysis bio-oils that contain large amounts of oxygenated molecules such as carboxylic acids, aldehydes, and alcohols into hydrocarbons for transportation fuels.[1] The ideal catalytic HDO process involves the removal of oxygen from the oxygenated molecules by selectively breaking the C−O bond without hydrogenating the unsaturated C═C and/or rupturing the saturated C−C bonds. Currently, typical industrial HDO processes have been carried out at moderate temperature range (300−600 °C) and high hydrogen pressure conditions using sulfided CoMo- and NiMo-based hydrotreating catalysts.[1−3] These hydrotreating catalysts, however, suffer from the rapid deactivation by coke formation and water poisoning,[3,4] and the incorporation of sulfur to keep the catalysts in the sulfided form poses downstream separation challenges. Recently, zeolite supported transition metals such as Pd and Raney Ni have been found to be very effective for phenol HDO in the aqueous phase.[5−8] However, the high pressure and large H_2 quantities required for traditional HDO hydrotreating catalysts (CoMo and NiMo) and for zeolite-based HDO in the aqueous phase dramatically increase the operating cost of the HDO process. Therefore, developing new catalysts for HDO with minimal hydrogen usage is highly desired. Considering the strong interaction between early transition metals such as Mo, W, and Ti and the oxygen atom, a two-stage deoxygenation process of oxygenates involving the oxidation followed by reduction of early transition metals could be achieved using a chemical looping process.[9] In the first stage, the oxygen atoms in oxygenate molecules are stripped off using mono- (or bi-) early transition metal catalysts. Then the oxygen-covered or formed metal oxide catalysts will be regenerated under reducing (or inert depending on the metal oxide) conditions by removing the oxygen and possible cokes.

Compared with other metal−oxygen bonds, the stronger Mo−O bond relative to the C−O bond of oxygenates suggests that Mo is one of potential deoxygenation catalyst without disturbing the C−C or the C═C bond.[10] A number of experimental studies of alcohol deoxygenation reactions on the clean and the modified Mo(110) surfaces had been reported by

Received: January 3, 2012
Revised: February 15, 2012
Published: February 16, 2012

Friend's group.[10−19] For example, Wiegand et al. studied the reactivity of 1-propanol on Mo(110) using the temperature-programmed desorption (TPD) technique.[20] Three competing decomposition pathways were found for the 1-propoxide intermediate after the initial O−H bond scission of 1-propanol. Propene was formed as the major product via deoxygenation and dehydrogenation, and propane was also formed via the C−O bond hydrogenolysis. In these two selective deoxygenation paths, the C−O bond scission was found to be the rate-limiting step. The third path involved complete dissociation of all bonds in acetaldehyde and led to the deposition of oxygen and carbon atoms on the Mo(110) surface and release of hydrogen in the gas phase. At the maximum coverage of 1-propoxide, the selective deoxygenation paths are slightly favored over the unselective complete decomposition path.[20] In another study, Chen and Friend found that the existence of oxygen overlayer (<0.5 ML) on the Mo(110) surface dramatically increases the selectivity to ethylene (C_2H_4) during ethanol decomposition.[10] They suggested that the oxygen-covered Mo(110) surface can inhibit the nonselective C−H bond scission of ethanol because of the modification of surface electronic structure by oxidation. The C−O bond scission is more facile on Mo compared with other transition metal surfaces. Previous experimental observations also suggested that ethylene production from ethylene glycol proceeds via a direct intermolecular elimination pathway by the C−O bond scission on the Mo(110) surface because of the strong Mo−O bond strength.[21]

Acetaldehyde (CH_3CHO) is the simplest model molecule of aldehydes with C═O, C−H, and C−C bonds. Fundamental understanding of CH_3CHO decomposition chemistry on the well-defined Mo(110) surface, particularly the cleavage preferences for the C═O, the C−H, and the C−C bonds of CH_3CHO is crucial in the development of new effective catalysts used for the first stage of the two-stage deoxygenation process mentioned above. Up to now, no experimental study of CH_3CHO adsorption and reaction on Mo(110) has been reported. Zhao et al. studied the adsorption and decomposition of CH_3CHO on the Pt(111) and Sn/Pt(111) surfaces using TPD.[22] At low coverage, they found that the adsorbed CH_3CHO irreversibly decomposes into the final products of CO, H_2, and CH_4 with some carbon deposition. With alloying Sn onto Pt(111) surface, the adsorption of CH_3CHO becomes reversible, and CH_3CHO decomposition would not occur during TPD. Davis and Barteau investigated CH_3CHO reaction on the clean Pd(111) surface.[23] They observed that the decomposition of adsorbed CH_3CHO via acetyl (CH_3CO), and the C−H bond scission is the rate-limiting step for the decarbonylation of CH_3CO intermediate.[23] Shekhar et al. further suggested that the CH_3CHO decomposition reaction on Pd is structure-sensitive using the isotopic-labeling technique.[24] Instead of first breaking the C−H bond on Pd(111), the C−C scission of CH_3CO proceeds before the C−H bond cleavage on Pd(110).

Density functional theory (DFT) calculations have been extensively used for gaining fundamental insights into the catalytic reactivity and plausible reaction mechanism on well-defined model catalyst surfaces.[25] However, very few of DFT studies on the adsorption and possible bond scissions of CH_3CHO on the transition metal surfaces are available in the literature.[26−28] Alcala et al. investigated the C−C and C−O bond cleavages of a series of reaction intermediates during ethanol decomposition on Pt(111) using periodic self-consistent DFT calculations.[26] Delbecq and Vigne also studied various adsorption geometries of CH_3CHO on Pt(111) and Pt/Sn(111) surfaces.[28] They found that CH_3CHO prefers to adsorbs at the bridge site in the η^2(C,O) configuration. To the best of our knowledge, no DFT study of adsorption and decomposition mechanism of CH_3CHO on the Mo(110) surface has been reported.

The essential function of a good deoxygenation catalyst is its ability to activate the C−O bond without breaking C−C or C−H bonds of oxygenate molecules. After the deoxygenation reaction, only oxygen O atom(s) is removed from the target oxygenate molecule without fragmentation and loss of energy value in terms of H atoms. For the ideal deoxygenation reaction of CH_3CHO on the Mo(110) surface, it is highly desired that the surface is oxidized by the oxygen atoms which is stripped from the adsorbed CH_3CHO. Concurrently, one of H atoms from the terminal methyl (CH_3) group of CH_3CHO transfers to the methylidyne (CH), releasing C_2H_4 into the gas phase as the final product. This implies that the selective deoxygenation of CH_3CHO to C_2H_4 not only involves the dehydrogenation with the C−H bond breaking but also the hydrogenation with the C−H bond making. It is expected that the accumulated surface oxygen atoms will convert the clean Mo(110) surface to the oxygen covered Mo(110) surface, and eventually to the MoO_x surface after the selective deoxygenation pathway.

The objective of the present work is to complement our previous theoretical investigation of acetaldehyde deoxygenation on the MoO_3(010) surface[29] and ongoing experimental efforts. Combining the novel dimer searching method[30] with extensive DFT calculations, various reaction pathways in CH_3CHO decomposition on the clean Mo(110) surface are identified in an unbiased way. The reaction mechanism network of CH_3CHO decomposition on Mo(110) obtained from this work will help us to develop selective Mo-based catalysts for the upgrading of bio-oil.

2. COMPUTATIONAL METHODOLOGY

All calculations were performed using spin-polarized DFT within the generalized gradient approximation (GGA) as implemented in the Vienna ab initio simulation package (VASP).[31−33] The core and valence electrons were represented by the projector augmented wave (PAW) method with a kinetic cutoff energy of 400 eV.[34,35] The exchange correlation functional was described by the Perdew−Burke−Ernzerhof (PBE) functional.[36] The ground-state atomic geometries of clean and the adsorbed Mo(110) systems were obtained by minimizing the forces on each atom to below 0.05 eV/Å.

The Mo bulk metal has a closed-packed body center cubic structure. Among three low-index surface structures, that is, (100), (111), and (110), the Mo(110) surface is the most stable structure with the lowest surface energy.[37] The optimized lattice constant of the Mo bulk is 3.158 Å using (9 × 9 × 9) Monkhorst−Pack (MP) mesh, which is in good agreement with the reported experimental value of 3.15 Å.[38] A periodic (3 × 3) supercell Mo(110) surface slab with four atomic layers was used in this work. During the geometric optimizations and the transition state searching processes, the adsorbate(s) and the Mo atoms in the top two surface layers were allowed to relax while the Mo atoms in the bottom two surface layers of the surface slab were fixed. A 15 Å vacuum layer was inserted between the Mo(110) surface slabs in the z direction to avoid interaction between images. To ensure the accuracy of calculations, the effects of slab thickness (up to six atomic layers) and different MP mesh sampling were tested. A (3 × 3

dx.doi.org/10.1021/cs3000039 | ACS Catal. 2012, 2, 468−478

× 1) MP sampling schedule was found to be accurate to reach total energy convergence of <0.02 eV. The adsorption energy, E_{ad}, of an adsorbate on the Mo(110) surface was calculated using the following definition

$$E_{ad} = E_{adsorbate+surface} - (E_{surface} + E_{adsorbate}) \quad (1)$$

where $E_{absorbate+surface}$ is the total energy of the adsorbate interacting with the surface slab; $E_{surface}$ is the total energy of the optimized surface slab; and $E_{absorbate}$ is the total energy of the adsorbate in vacuum. A negative E_{ad} value indicates favorable (exothermic) adsorption.

In this work, the transition and final states of each reaction path involved one of possible bond cleavages of the adsorbed CH_3CHO and subsequent reaction intermediates during decomposition were identified using the minimum-mode following the dimer method.[30] The dimer searching method principally is different from the traditional nudged elastic band (NEB) searching method in which both the initial and the final states have to be determined before locating the transition state in the reaction path. In the dimer searching method, only the initial state of the adsorbed molecule is needed. Both the transition and the final states are located automatically. Therefore, the dimer searching method allows us to explore the unbiased reaction mechanism without prior knowledge of the possible final state (product).

Starting with a stable initial configuration of the adsorbed molecule, two configurations (a dimer) are created by making two equal and opposite small finite-difference displacements (0.05 Å) in the coordinates of the adsorbed molecule. Then the dimer is driven to the saddle point (i.e., the transition state) by iteratively and alternatively taking rotation and translation steps. Both rotation and translation steps are implemented with a conjugate gradient optimizer. After locating the transition state (saddle point), the dimer images (structures) are displaced from the saddle point along the negative mode by 0.01 Å and then relaxed to the neighboring local minima. In a successful search, one of the images will minimize to the initial state, and the other will be in a new (second) final state. In this work, the tolerance for convergence to the transition state was such that the force on each atom was less than 0.02 eV/Å.[30] The identified transition state in each dimer search has also been further confirmed as being first-order saddle point using a finite-difference normal-mode analysis. Only one imaginary frequency is obtained at the transition state. The reaction energy is calculated as the total energy difference between the final state and the initial state. The forward and reverse activation barriers for each reaction path are defined as the total energy difference between the initial state and the transition state, and between the final state and the transition state, respectively. We have successfully used the dimer searching method to explore the unbiased reaction mechanisms of methanol decomposition and CO_2 hydrogenation to methanol on Cu surfaces,[39−42] as well as acetaldehyde deoxygenation on the MoO_3(010) surface.[29]

The zero-point energy (ZPE) effect on the adsorption energies and reaction energetics was checked. Harmonic ZPE correction was calculated on the basis of vibrational frequencies of initial, transition, and final states. We found that ZPE correction only contributes a very small reduction in the activation barrier, as well as the reaction energy for each identified reaction pathway (<0.1 eV). Therefore, we do not include the ZPE corrections in the energies reported in this work.

3. RESULTS AND DISCUSSION

Four high symmetric adsorption sites, that is, atop, short-bridge, long-bridge, and pseudo 3-fold hollow sites are available on the Mo(110) surface (Figure 1). Herein the adsorption

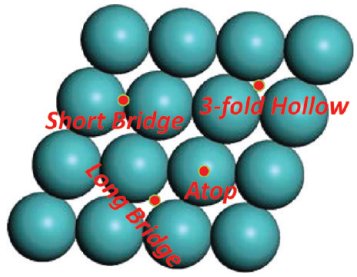

Figure 1. Top view of symmetric adsorption sites on the p(3 × 3) supercell Mo(110) surface.

configuration of each intermediate is designated as the $\eta^i\mu_j$ nomenclature that indicates the number of atoms (i) of adsorbed species is bonded with the number of Mo surface atoms (j). Various adsorption configurations and sites for key reaction intermediates have been identified. Two most distinguishable configurations (η^1 and η^2) at 1/9 monolayer (ML) coverage are summarized in Table 1 and Figure 2. It also has to be mentioned that only the most likely reaction path with the lowest activation barrier for each bond breaking step will be discussed in detail below although multiple paths for the same elementary step are identified using the dimer searching method.

3.1. Adsorption and Decomposition of CH_3CHO. Two distinctive stable adsorption configurations of CH_3CHO are found on the clean Mo(110) surface. As shown in Figure 2a and 2b, CH_3CHO binds either at the atop site via a single Mo−O bond, that is, in the $\eta^1\mu_1$(O) configuration or at the pseudo 3-fold hollow site in the $\eta^2\mu_3$(C,O) configuration. For the $\eta^1\mu_1$(O) configuration, CH_3CHO adsorbs on Mo(110) through the oxygen lone pair orbital while the bonding occurs through the carbonyl π orbital with back-donation from the Mo surface in the $\eta^2\mu_3$(C,O) configuration, consistent with previous reports.[28,43] The calculated adsorption energies of CH_3CHO at the atop and the hollow sites are −0.73 and −1.91 eV, respectively. This indicates that the adsorbed CH_3CHO in the $\eta^2\mu_3$(C,O) configuration is much more stable than it is in the $\eta^1\mu_1$(O) configuration. We note that this adsorption preference of CH_3CHO is different from that on other transition metal surfaces such as Pt, Pd, and Rh. It was found that $\eta^1\mu_1$(O) configuration of CH_3CHO is slightly (0.1 eV) more favorable than the $\eta^2\mu_3$(C,O) configuration on Pt, Pd, and Rh was found in previous experiments[22,24,44] and theoretical studies.[26−28]

CH_3CHO decomposition can be activated by breaking one of four bonds (β-C−H, γ-C−H, C−O, and C−C). There are two types of C−H bond (β-C−H and γ-C−H) scissions of the adsorbed CH_3CHO that lead to two different products. The β-C−H bond scission yields CH_3CO while the γ-C−H bond scission generates formylmethyl (CH_2CHO). In the β-C−H bond scission of CH_3CHO, the C−H bond breaks along the long-bridge direction on the Mo(110) surface. The dissociated H atom moves across the atop site of Mo atom. At the final state, both CH_3CO and atomic H bind at the pseudo 3-fold hollow site (Figure 3a). The calculated activation barrier for the β-C−H bond scission is 0.29 eV with a reaction energy of

dx.doi.org/10.1021/cs3000039 | ACS Catal. 2012, 2, 468−478

Table 1. Calculated Adsorption Energies (E_{ad}) and the Geometric Parameters of Reaction Intermediates on Mo(110)

species	site	configuration	bond length (Å)	E_{ad} (eV)
CH_3CHO	atop	$\eta^1\mu_1$(O)	d(Mo−O) = 2.064	−0.73
	hollow	$\eta^2\mu_3$(C,O)	d(Mo−O) = 2.099; 2.223	−1.91
			d(Mo−C) = 2.337	
CH_2CHO	short-bridge	$\eta^2\mu_2$(C,O)	d(Mo−O) = 2.259	−2.90
			d(Mo−C) = 2.027	
	hollow	$\eta^3\mu_3$(C,C,O)	d(Mo−O) = 2.129; 2.224	−3.47
			d(Mo−C) = 2.283; 2.275	
CH_3CO	atop	$\eta^1\mu_1$(O)	d(Mo−O) = 2.068	−1.60
	hollow	$\eta^2\mu_3$(C,O)	d(Mo−O) = 2.189; 2.290; 2.291	−3.57
			d(Mo−C) = 2.181; 2.234; 2.338	
CH_2CO	short-bridge	$\eta^1\mu_2$(O)	d(Mo−O) = 2.343; 2.355	−0.08
	hollow	$\eta^2\mu_3$(C,O)	d(Mo−O) = 2.136; 2.247	−2.44
			d(Mo−C) = 2.141; 2.227	
CH_3CH	hollow	$\eta^1\mu_3$(C)	d(Mo−C) = 2.153; 2.187; 2.331	−4.53
C_2H_4	atop	$\eta^2\mu_1$(C, C)	d(Mo−C) = 2.270; 2.274	−1.66
CH_3C	hollow	$\eta^1\mu_3$(C)	d(Mo−C) = 2.084; 2.085; 2.362	−6.28
CH_2CH	hollow	$\eta^2\mu_2$(C, C)	d(Mo−C) = 2.130; 2.302; 2.317	−3.77
CH_2C	hollow	$\eta^2\mu_3$(C,C)	d(Mo−C) = 2.112; 2.114; 2.192	−4.85
			d(Mo−C) = 2.376	
CHC	hollow	$\eta^2\mu_3$(C,C)	d(Mo−C) = 2.052; 2.182; 2.207	−6.64
			d(Mo−C) = 2.193; 2.247	
CO	hollow	$\eta^2\mu_3$(C,O)	d(Mo−C) = 1.976; 2.299; 2.324	−2.07
			d(Mo−O) = 2.322	
C	long-bridge	$\eta^1\mu_2$(C)	d(Mo−C) = 1.983; 1.983	−7.84
O	hollow	$\eta^1\mu_3$(O)	d(Mo−O) = 2.037; 2.037; 2.108	−4.59[a]
H	hollow	$\eta^1\mu_3$(H)	d(Mo−H) = 1.939; 2.026; 2.029	−0.85[a]

[a] E_{ad} of atomic O and H are relative to 1/2 E_{O_2} and 1/2 E_{H_2} in the gas.

−0.74 eV, indicating the β-C−H scission of CH_3CHO is very facile and energetically downhill. On the other hand, as the γ-C−H bond is activated (Figure 3b), the CH_3 group in the adsorbed CH_3CHO rotates and tilts down to the surface. At the transition state, the C−H bond distance is elongated from 1.10 to 1.56 Å. At the final state, the dissociated H atom binds at the neighboring hollow site while the remaining CH_2CHO group stays at the same 3-fold hollow site. Although the γ-C−H scission of CH_3CHO is still exothermic (−0.20 eV), the calculated activation barrier is 0.86 eV, which is much higher than the β-C−H scission barrier. Clearly, the dehydrogenation of the adsorbed CH_3CHO will proceed by breaking the β-C−H bond rather than the γ-C−H bond.

The C−O bond scission of CH_3CHO yields ethylidene (CH_3CH) and atomic oxygen. Different from the two dehydrogenation paths where the C−H bond activation proceeds by moving atomic H, the C−O bond breaking of CH_3CHO starts by moving CH_3CH instead of atomic oxygen because of the strong Mo−O bonding. The dissociated CH_3CH group moves from the hollow site to the neighboring short-bridge site while the atomic oxygen stays at the initial hollow site. The C−O bond is elongated to 2.62 Å at the transition state (Figure 3c). At the final state, the dissociated CH_3CH binds at the hollow site in the $\eta^2\mu_3$(C,C) configuration. The activation barrier for the C−O bond scission of CH_3CHO is 0.45 eV. The calculated reaction energy is −1.51 eV, showing that the C−O bond scission of CH_3CHO is highly exothermic.

The C−C bond of CH_3CHO can also be broken generating a methyl group and a formyl (CHO) group. As shown in Figure 3d, the CHO seems to stay at the original binding site but the CH_3 moves to the neighboring short-bridge site as the C−C bond of CH_3CHO breaks. The C−C bond distance is only elongated from 1.50 to 1.86 Å at the transition state. This implies the activation of the C−C bond scission is an early transition state. At the final state, the CHO group binds at the hollow site in the $\eta^2\mu_3$(C,O) configuration and the CH_3 group binds at the short-bridge site through the carbon atom. The C−C distance at the final state is 4.24 Å. The calculated C−C bond activation barrier is 1.30 eV with a reaction energy of −0.29 eV.

Compared with all four bond scissions of CH_3CHO, it can be concluded that the β-C−H and the C−O bond scissions of CH_3CHO precede the γ-C−H and the C−C bond scissions. Also, we note that both the β-C−H and the C−O bond scissions of CH_3CHO are most likely irreversible because of the large exothermicity. Although the β-C−H scission is slightly preferred to the C−O bond scission, it is expected these two elementary steps are competitive. The initial decomposition of the adsorbed CH_3CHO on the clean Mo(110) surface leads to either CH_3CO or CH_3CH.

3.2. CH_3CO Decomposition. Acetyl had been spectroscopically observed in previous TPD experiments of CH_3CHO on transition metal surfaces such as Pd,[23,24] Pt,[22,45] and Rh.[44] Similar to the CH_3CHO adsorption, two stable adsorption configurations of CH_3CO on the Mo(110) surface were found. The optimized Mo−O and Mo−C bond lengths in both configurations are almost the same as the corresponding bond lengths of the adsorbed CH_3CHO. Our calculations show that the adsorbed CH_3CO in the $\eta^2\mu_3$(C,O) configuration (−3.57 eV) is much more stable than its adsorption in $\eta^1\mu_1$(O) configuration (−1.60 eV).

Starting from the most stable $\eta^2\mu_3$(C,O) configuration (Figure 2e), three possible reaction paths for the adsorbed CH_3CO on Mo(110) are identified. As shown in Figure 4a, the γ-C−H cleavage of CH_3CO generating ketene (CH_2CO) species is similar to the γ-C−H cleavage of CH_3CHO, but with a lower activation barrier (0.66 eV). The γ-C−H cleavage of CH_3CO is energetically neutral (+0.02 eV). The second decomposition path of CH_3CO is via the C−O bond scission leading to the formation of ethylidyne (CH_3C). The calculated activation barrier for the C−O bond scission is 0.37 eV, which is lower than the barrier for the γ-C−H bond scission, indicating the C−O scission of CH_3CO is preferred to the γ-C−H bond scission. It was also noted that the dimer searching method used in this work only identified an Eley−Rideal reaction path for the C−C bond scission of CH_3CO. We could not rule out the possibility of this C−C bond scission via the common Langmuir−Hinshelwood mechanism because of the limited number of dimer searching. Instead of producing an

dx.doi.org/10.1021/cs3000039 | ACS Catal. 2012, 2, 468−478

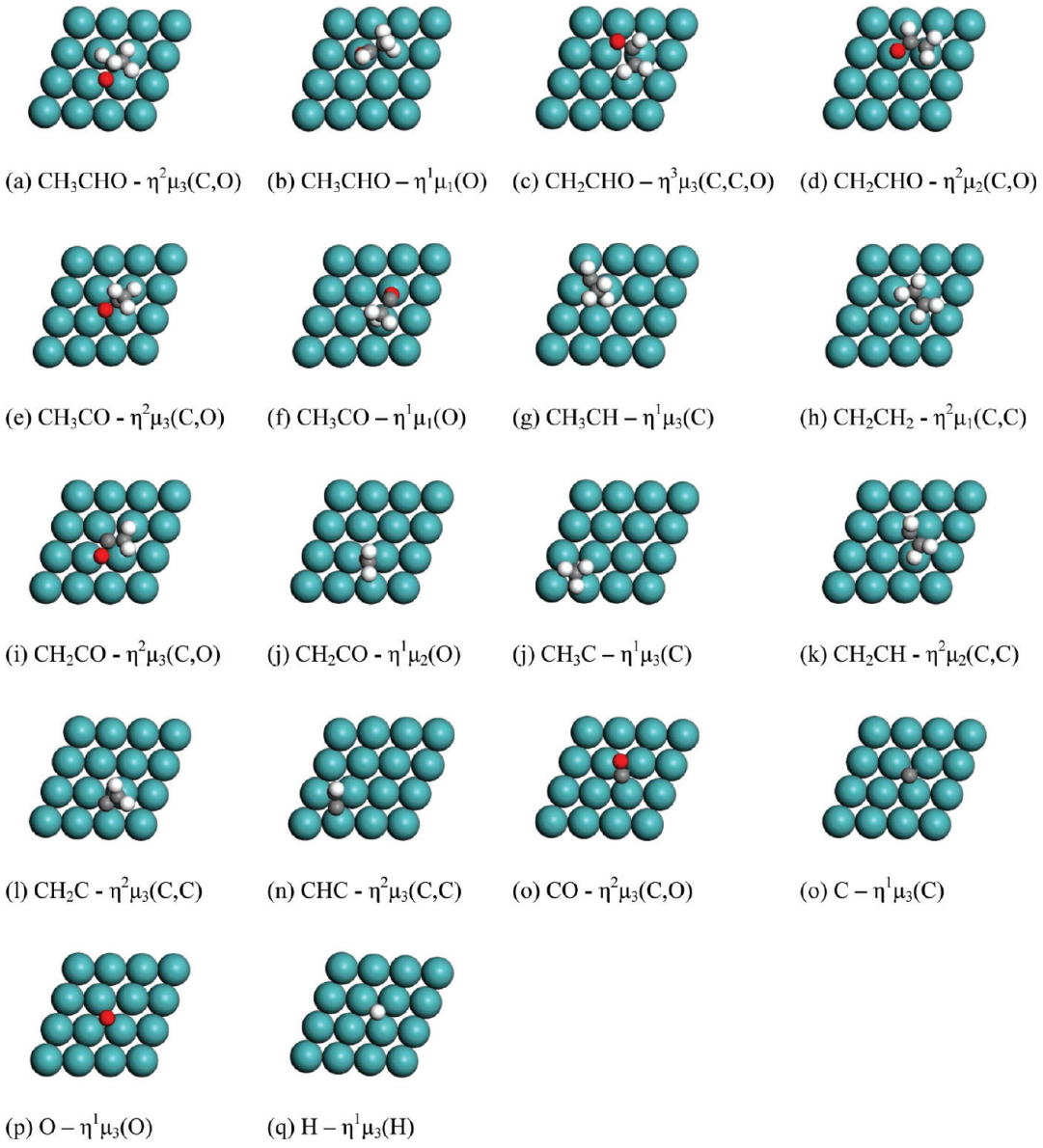

Figure 2. Top views of optimized geometries of adsorbed reaction intermediates on Mo(110). Mo atoms are in light blue; O atom is in red, C atoms are in dark gray; H atoms are in white.

adsorbed CO on the surface, only the methyl group is bound at the hollow site while CO was released into the gas phase. We found that the C−C bond cleavage of CH_3CO is exothermic (−0.86 eV) with an activation barrier of 0.83 eV, which is higher than the activation barriers of the C−O and the γ-C−H bond scissions. This suggests that the C−C bond cleavage of CH_3CO on Mo(110) is unlikely. As a result, in contrast to CH_3CHO decomposition on transition metal surfaces where CO is a major product from acetyl decarbonylation,[22−24,44−46] the decarbonylation of acetyl on the Mo(110) surface is, at most, a minor reaction path.

3.3. CH_3CH Decomposition. CH_3CH is the possible reaction intermediate resulting from the initial decomposition of CH_3CHO via the C−O bond cleavage. CH_3CH prefers to bind at the hollow site in the $\eta^1\mu_3$(C) configuration through the carbon atom (Figure 2g). The calculated adsorption energy of CH_3CH at the hollow site is −4.53 eV. Except for the C−C bond scission, which we found it is unlikely due to the high endothermicity of +1.32 eV, two types of the hydrogen abstraction (β and γ) of CH_3CH leading to the formation of CH_3C and vinyl (CH_2CH) are possible. Our calculations show that the activation barriers for the β- and the γ-C−H scissions are 0.24 and 0.31 eV, respectively. This indicates that both dehydrogenation steps of CH_3CH are rapid and competitive. Our calculations show the dehydrogenation reactions of CH_3CH are exothermic (−0.53 and −0.38 eV). As shown in Figure 5a, the γ-C−H bond scission of CH_3CH begins with the CH_3 group tilting down to the surface. At the transition state, the C−H bond is already broken. The methylene group (CH_2) actually binds at the atop Mo site and the dissociated H atom moves to the short-bridge site. The C−H distance is 0.23 Å longer than its equilibrium distance of 1.16 Å. For the β-C−H bond scission of CH_3CH, only the atomic H moves away from the CH_3C, which still sits at the hollow site. In terms of the C−H distances at the transition states, both C−H bond scissions of CH_3CH have early transition states.

3.4. CH_2CHO Decomposition. Compared with the C−O and the β-C−H cleavages, the γ-C−H scission of CH_3CHO

dx.doi.org/10.1021/cs3000039 | ACS Catal. 2012, 2, 468−478

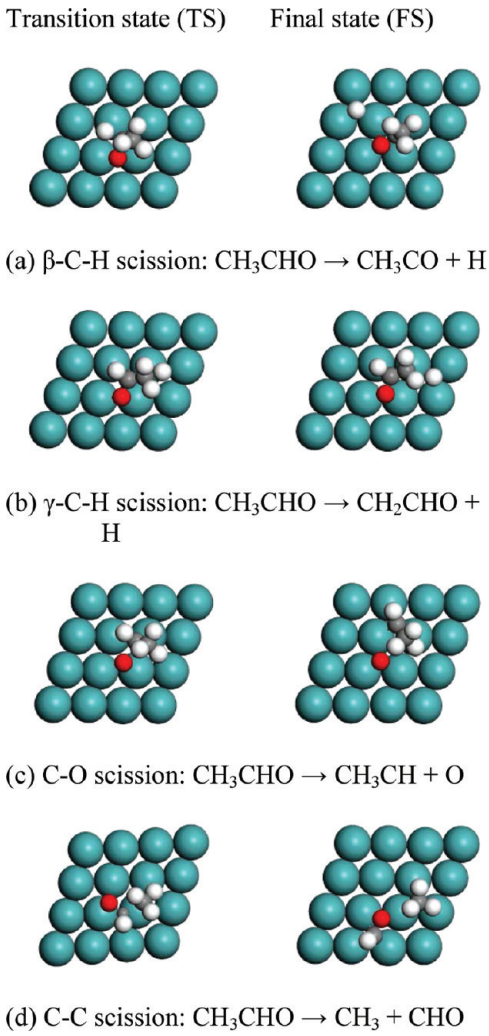

Figure 3. Top views of transition state (TS) and final state (FS) structures for CH_3CHO decomposition. The same color scheme in Figure 2 is applied.

leading to the formation of CH_2CHO is kinetically unfavorable because of the high activation barrier. It is reasonably postulated that the γ-C−H scission of CH_3CHO is only a minor reaction path for CH_3CHO decomposition on Mo(110), which might occur at high temperature conditions. Two stable adsorption configurations of CH_2CHO were found. Different from the η^2 configuration which is identified as the most stable configuration for other intermediates, it is found that the most stable adsorption configuration of CH_2CHO on the Mo(110) surface is a η^3 configuration via the triple bonds, that is, two Mo−C bonds and one Mo−O bond. CH_2CHO adsorbs at the pseudo 3-fold hollow site in the $\eta^3\mu_3$(C,C,O) configuration (Figure 2c) which is 0.57 eV stronger than its bonding at the short-bridge site in the $\eta^2\mu_2$(C,O) configuration (Figure 2d).

Figure 6 shows the transition and final states of three dissociation paths via one of three possible bond cleavages (β-C−H, C−O, C−C) of CH_2CHO. We found that the β-C−H scission of CH_2CHO on Mo(110) is very similar to the β-C−H scission of CH_3CHO. The dissociated H atom initially moves across the atop Mo site at the transition state, then binds at the hollow site at the final state. The formed ketene (CH_2CO) species stays at the original hollow site in the $\eta^2\mu_2$(C,O) configuration. A similar low activation barrier of 0.35 eV for the

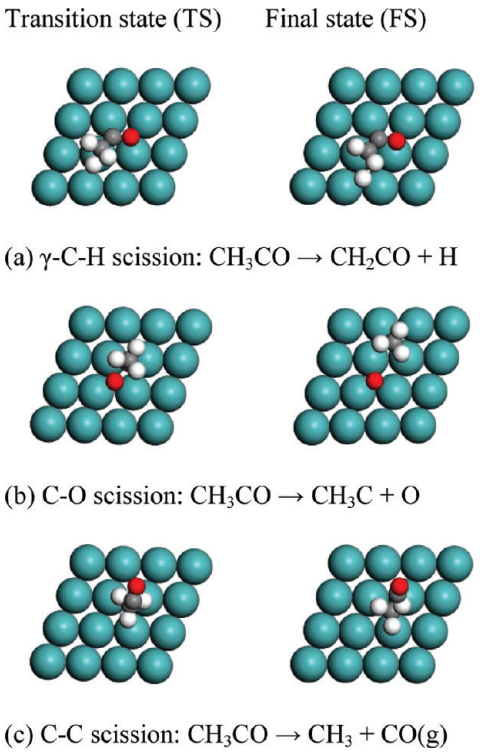

Figure 4. Top views of transition state (TS) and final state (FS) structures for CH_3CO decomposition. The same color scheme in Figure 2 is applied.

β-C−H scission of CH_2CHO is found. The calculated reaction energy of the β-C−H scission of CH_2CHO is −0.44 eV. The C−O scission of CH_2CHO produces vinyl. We found that the C−O bond scission of CH_2CHO is also very similar to the C−O scission of CH_3CHO. The activation barrier and reaction energy are 0.52 and −1.43 eV for the C−O scission of CH_2CHO, which is very close to the reaction energetics for the C−O scission of CH_3CHO (0.45 and −1.51 eV). Obviously, the vinyl formation from methylformyl deoxygenation is irreversible. The C−C bond breaking of CH_2CHO generating a formyl group and a methylene group is shown in Figure 6c. The C−C bond is already broken with a distance of 1.99 Å at the transition state. Both formyl and methylene groups depart each other during the C−C bond activation. Compared with the β-C−H and the C−O bond scissions, our calculation show the C−C cleavage of CH_2CHO is unlikely due to the high activation barrier (0.98 eV). We note that the barrier for the C−C bond breaking of CH_2CHO is dramatically lower than the barrier for the C−C cleavage of CH_3CHO. This can be rationalized by the $\eta^3\mu_3$(C,C,O) configuration of the adsorbed CH_2CHO. With two carbon atoms of CH_2CHO binding with the surface Mo atoms forming two strong Mo−C bonds, the C−C bond of CH_2CHO becomes weaker. Consequently, the C−C bond scission of CH_2CHO is easier than the C−C cleavage of CH_3CHO which has only one Mo−C bond. In summary, it is expected that CH_2CHO decomposition results in either ketene or vinyl by the β-C−H or the C−O bond scission.

3.5. CH_2CO Decomposition. Ketene can be formed by the dehydrogenation of either formylmethyl or acetyl. On the Mo(110) surface, ketene prefers to adsorb at the hollow site in the $\eta^2\mu_3$(C,O) configuration (Figure 2i) with an adsorption energy of −2.44 eV. Of three decomposition paths via the γ-C−

dx.doi.org/10.1021/cs3000039 | ACS Catal. 2012, 2, 468−478

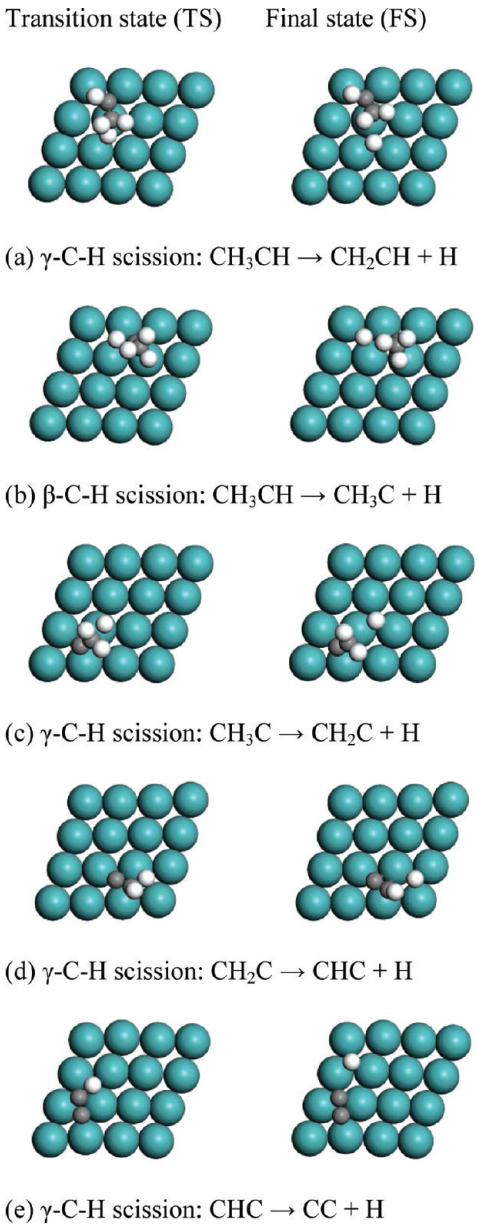

Figure 5. Top views of transition state (TS) and final state (FS) structures for CH_3CH, CH_3C, and CH_2C decomposition. The same color scheme in Figure 2 is applied.

H, the C−O and the C−C bond scissions of ketene shown in Figure 7, the C−O bond scission of CH_2CO is found highly exothermic (−1.66 eV) with a low activation barrier of 0.33 eV. While the barriers for the γ-C−H and the C−C cleavages of CH_2CO are 0.82 and 1.31 eV, respectively. Therefore, the γ-C−H and the C−C bond cleavages of CH_2CO are improbable. The decomposition of ketene most likely leads to the formation of vinylidene (CH_2C). Interestingly, the calculated barrier for the C−C bond scission of ketene is 1.30 eV, which is almost the same as the barrier for the C−C bond cleavage of CH_3CHO (1.31 eV), but higher than the C−C activation barrier of CH_2CHO (0.98 eV). Again, this is largely due to the similar $\eta^2\mu_3$(C,O) configuration for both CH_2CO and CH_3CHO while CH_2CHO adsorbs at the Mo(110) surface in the $\eta^3\mu_3$(C,C,O) configuration.

3.5. Ethylene Formation. The objective of this work is to explore the deoxygenation possibility of selectively converting

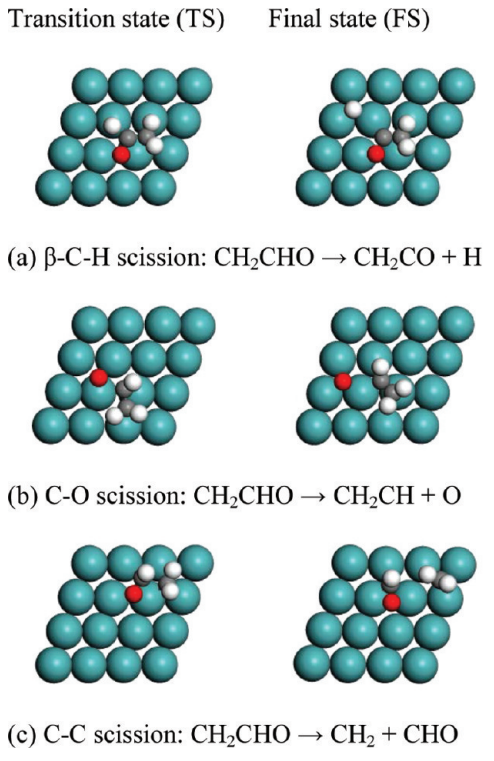

Figure 6. Top views of transition state (TS) and final state (FS) structures for CH_2CHO decomposition. The same color scheme in Figure 2 is applied.

acetaldehyde to ethylene on the Mo(110) surface. Vinyl is formed by either ethylidene dehydrogenation or formylmethyl

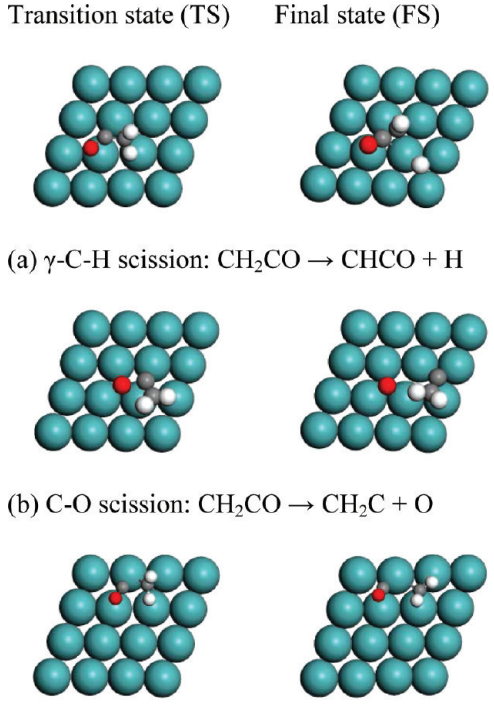

Figure 7. Top views of transition state (TS) and final state (FS) structures for CH_2CO decomposition. The same color scheme in Figure 2 is applied.

dx.doi.org/10.1021/cs3000039 | ACS Catal. 2012, 2, 468−478

deoxygenation. With atomic H nearby, vinyl can be further hydrogenated into ethylene. At the initial state, both atomic H and vinyl bind at the neighboring hollow sites. The distance between carbon atom of vinyl and atomic H is 2.40 Å. Then both the atomic H and vinyl move toward the atop site between the two hollow sites. As shown in Figure 8b, the C−H distance

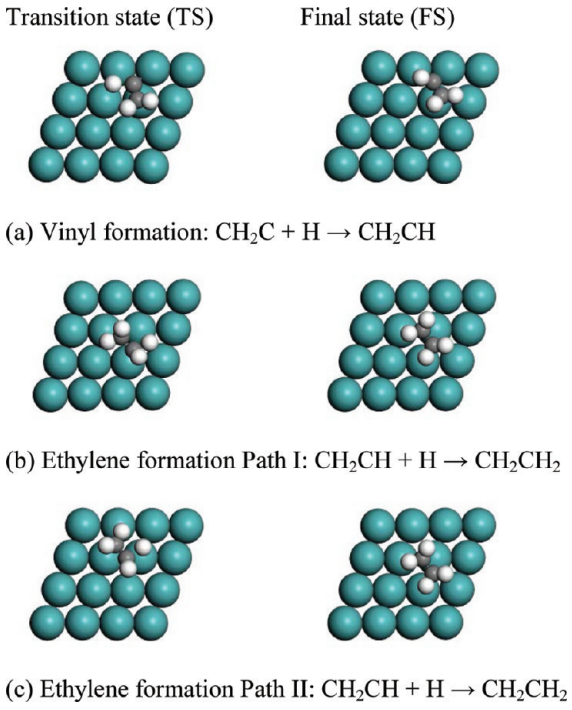

Figure 8. Top views of transition state (TS) and final state (FS) structures for ethylene formation by hydrogenation steps. The same color scheme in Figure 2 is applied.

becomes 1.41 Å at the transition state. The formed ethylene binds at the atop Mo site in the $\eta^2\mu_1$(C,C) configuration. In this π adsorption structure, two carbon atoms of ethylene bind at the same Mo atom with the Mo−C bond length of 2.27 Å. The calculated ethylene formation barrier is 0.62 eV. On the other hand, we note that vinyl can alternatively be hydrogenated back to ethylidene, that is, the reverse reaction of ethylidene decomposition via the C−H bond scission. The barrier for ethylidene formation from vinyl hydrogenation is 0.69 eV, indicating the two vinyl hydrogenation paths toward ethylene and ethylidene are competing.

Consistent with previous experimental observation,[47] the interaction between ethylene and Mo(110) is strong. The calculated adsorption energy of ethylene at the atop site of the Mo(110) surface is −1.66 eV. Because the vinyl hydrogenation to ethylene is thermodynamically neutral with a reaction energy of −0.02 eV, the formed ethylene prefers to dissociate back to vinyl and atomic H with a barrier of 0.64 eV instead of desorbing from the surface. However, our calculation also suggests that there is a strong repulsive interaction (0.5 eV) between the coadsorbed surface oxygen atom and ethylene. The interaction between ethylene and the Mo(110) surface becomes weaker with the increasing surface oxygen accumulation. This is supported by previous experimental results.[47] For example, Frühberger and Chen found that ethylene interacts with the oxygen precovered Mo(110) surface very weakly. After heating, the weakly bound ethylene species desorb without significant amount of decomposition.[47] In our previous study of acetaldehyde deoxygenation on the MoO_3(010) surface, we also found that ethylene desorption from the Mo═O terminal is almost spontaneous. It is expected that ethylene could desorb from the oxygen covered Mo(110) surface upon acetaldehyde decomposition.

3.6. Nonselective Reaction Paths to Hydrocarbon Fragments. Further dehydrogenation of ethylidyne and vinyl produces vinylidene (CH_2C). In the C−H bond scission of CH_3C, the adsorbed CH_3C at the hollow site first moves to the long-bridge site and tilts down to the surface. The C−H distance of methyl is elongated from 1.10 Å at the initial state to 1.61 Å at the transition state (Figure 5c). At the final state, the formed CH_2C adsorbs the long-bridge site and the dissociated H atom binds at the neighboring hollow site.

Compared to the vinyl hydrogenation, vinyl dehydrogenation via the β-C−H bond scission producing vinylidene is kinetically favorable. The barrier for the β-C−H bond scission of vinyl is only 0.20 eV, which is lower than the hydrogenation barriers discussed above. The calculated reaction energy of vinyl dehydrogenation to vinylidene is −0.04 eV, suggesting this β-C−H bond scission step is facile and reversible. The produced vinylidene is not stable and is quickly converted to ethynyl (CHC) on the Mo(110) surface because the calculated dehydrogenation barrier is only 0.08 eV. Finally, the further dehydrogenation of CHC leads to the accumulation of surface carbon atoms. As shown in Figure 5e, the two bonded carbon atoms bind at neighboring hollow sites with a C−C distance of 1.38 Å, and the atomic H drifts away from two carbon atoms. However, our result shows the barrier for this final dehydrogenation step is high (1.00 eV).

The linear scaling relationship between the activation barrier and the reaction energy for a given elementary reaction step on transition metal and metal oxide surfaces have been extensively explored.[48−50] This so-called Brønsted−Evans−Polanyi relationship is very useful because it allows us to estimate the activation barrier of the specific elementary step using the adsorption energies of reactants and products or other energy references[51−54] without calculating the transition state. For example, Loffreda et al. found a good linear relationship between the activation barriers and the total energy of initial precursor state for 32 elementary steps of acrolein hydrogenation on Pt(111).[53] In this work we found, however, that there is no linear correlation between the activation barriers and the reaction energies (or the energy of initial precursor states) for C−H, C−O, and C−C bond scissions. Instead, a somewhat linear relationship between the activation barrier (E_a) and the total energy (E_{FS})[54] of the reaction intermediate(s)/adsorbate(s) at the final state was located for each bond scission step. As shown in Figure 9, a good linear scaling relationship for the elementary steps with the C−O bond scission is found with a correlation coefficient of 0.999. For the C−H and C−C bond scission reactions, our calculation results seem to be too scattered to obtain a trustworthy linear relationship.

The complete reaction network of acetaldehyde decomposition on the clean Mo(110) surface is shown in Figure 10. For each bond-breaking or -making step, the lowest activation barrier and corresponding reaction energy of the path are listed. Except for the unlikely C−C bond scission, the acetaldehyde decomposition mechanism consists of many competing elementary reaction steps via both the C−O and the C−H bond scissions of various reaction intermediates (Table 2). Compared with the γ-C−H and the C−O bond scissions of the

dx.doi.org/10.1021/cs3000039 | ACS Catal. 2012, 2, 468−478

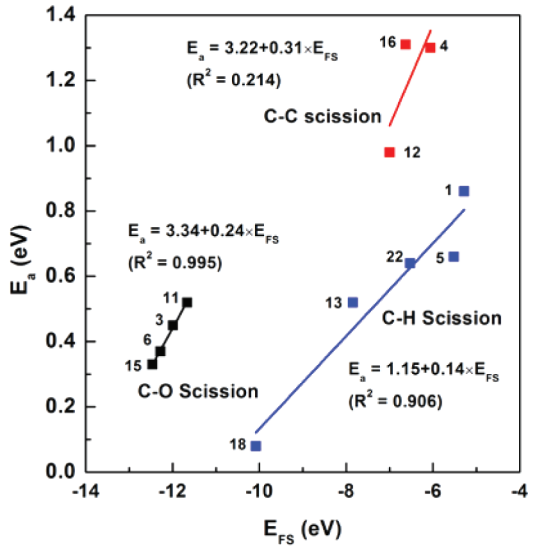

Figure 9. Correlation of the activation barriers and the final state energies for C−C, C−H, and C−O bond cleavages of CH_3CHO on the clean Mo(110) surface.

adsorbed CH_3CHO, the C−C and β-C−H bond scissions are least likely to occur because of the high activation barriers of 0.86 and 1.30 eV. The initial decomposition of CH_3CHO leads to either CH_3CO or CH_3CH. For the adsorbed CH_3CO, the deoxygenation into CH_3C is more favorable than its dehydrogenation into CH_2CO via the γ-C−H bond scission. Two dehydrogenation paths of CH_3CH leading to CH_3C and CH_2CH are competing. The resulting CH_3C and CH_2CH will further dehydrogenate into CH_2C, and then CHC species. As a result, the dominant reaction route for acetaldehyde decomposition on the Mo(110) surface is the nonselective path leading to atomic oxygen and ethynyl on the surface. The surface hydrogen atoms can recombine and release H_2 into the gas phase. This is consistent with the previous experiment that H_2 is a major product in ethylene decomposition on Mo(110).[47] Our results show that the removal of surface carbon deposition on the Mo(110) surface is difficult. The calculated CO formation barrier from the recombination of atomic C and O is 1.98 eV, indicating the CO formation is prohibited by the strong Mo−O and Mo−C interactions.

On the other hand, the selective reaction route of acetaldehyde decomposition leading to ethylene formation is the minor reaction path on Mo(110). It most likely proceeds as follows:

$$CH_3CHO \rightarrow CH_3CO + H$$
$$\rightarrow CH_3C + O + H$$
$$\rightarrow CH_2C + O + 2H$$
$$\rightarrow CH_2CH + O + H$$
$$\rightarrow CH_2CH_2 + O$$

This selective decomposition route is largely inhibited by the facile dehydrogenation of vinyl and vinylidene on the clean Mo(110) surface. We expect that the oxygen and/or carbon modified Mo (110) surfaces may shift the acetaldehyde decomposition path from the nonselective path to the selective path. For the selective deoxygenation of acetaldehyde to ethylene to be feasible in the absence of H_2, we need to identify a promoter that can facilitate the hydrogenation of vinyl/vinylidene and, similar to O and C covered Mo surface, weaken the interaction of ethylene with Mo.[47] In the context of typical HDO reaction conditions, we expect the high H_2 pressure would facilitate the vinyl hydrogenation (instead of the more favorable vinyl dehydrogenation in the absence of H_2) leading to deoxygenation of acetaldehyde to ethylene/ethane. A very similar deoxygenation path via CH_3CH, CH_2CH intermediates is competitive with the above path. Both deoxygenation routes are bottlenecked by the last elementary step, that is, the hydrogenation of vinyl to ethylene.

Finally, it is noteworthy that acetaldehyde decomposition reaction on Mo(110) differs from previous experimental observation on transition metal (Pd, Rh, Pt) surfaces. First of all, an interesting finding from the present work is that the decarbonylation of acetaldehyde on Mo(110) is unlikely. This is due to the much stronger Mo−O bond over the C−O bond. Instead of breaking the C−C bond of acetaldehyde, the C−O bond is cleaved first. Moreover, the strong Mo−O and Mo−C interactions also inhibit the CO formation from the atomic O and C on the surface. Second, unlike the hydrogenation ability of transition metals, the facile C−H bond scission (dehydrogenation) on the Mo(110) surface leads to the formation of

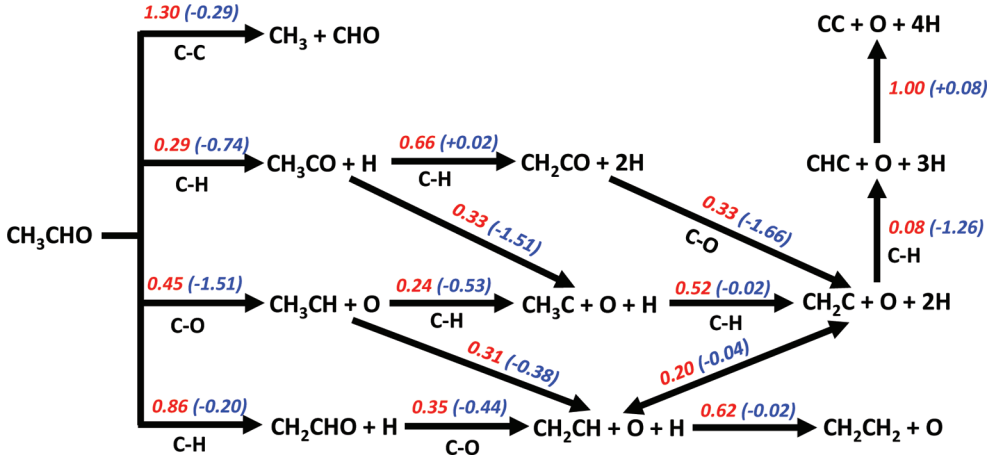

Figure 10. Reaction network of CH_3CHO decomposition on Mo(110). The activation barrier and reaction energy are listed in red and blue numbers, respectively.

dx.doi.org/10.1021/cs3000039 | ACS Catal. 2012, 2, 468−478

Table 2. Calculated Reaction Energies (ΔH) and Activation Barriers (E_a) of Elementary Reaction Steps

no.	elementary reaction	bond	ΔH (eV)	E_a (eV)	bond distance at IS, TS, and FS (Å)	imaginary frequency at TS (cm^{-1})
			Bond-Breaking			
1	$CH_3CHO \leftrightarrow CH_2CHO + H$	γ-C−H	−0.20	0.86	1.104; 1.563; 2.560	923
2	$CH_3CHO \leftrightarrow CH_3CO + H$	β-C−H	−0.74	0.29	1,174; 2.429; 3.495	487
3	$CH_3CHO \leftrightarrow CH_3CH + O$	C−O	−1.51	0.45	1.434; 2.619; 3.067	712
4	$CH_3CHO \leftrightarrow CH_3 + CHO$	C−C	−0.29	1.30	1.500; 1.863; 4.237	286
5	$CH_3CO \leftrightarrow CH_2CO + H$	γ-C−H	+0.02	0.66	1.110; 1.551; 2.664	784
6	$CH_3CO \leftrightarrow CH_3C + O$	C−O	−1.42	0.37	1.403; 1.784; 3.348	626
7	$CH_3CO \leftrightarrow CH_3 + CO(g)$	C−C	−0.86	0.83	1.481; 1.835; 3.880	358
8	$CH_3CH \leftrightarrow CH_3C + H$	β-C−H	−0.53	0.24	1.157; 1.543; 2.714	736
9	$CH_3CH \leftrightarrow CH_2CH + H$	γ-C−H	−0.38	0.31	1.162; 1.485; 2.662	917
10	$CH_2CHO \leftrightarrow CH_2CO + H$	β-C−H	−0.44	0.35	1.162; 1.596; 3.158	821
11	$CH_2CHO \leftrightarrow CH_2CH + O$	C−O	−1.43	0.52	1.391; 2.101; 2.901	646
12	$CH_2CHO \leftrightarrow CH_2 + CHO$	C−C	+0.03	0.98	1.451; 1.992; 3.786	345
13	$CH_3C \leftrightarrow CH_2C + H$	γ-C−H	−0.02	0.52	1.104; 1.607; 2.790	624
14	$CH_2CO \leftrightarrow CHCO + H$	γ-C−H	−0.87	0.82	1.095; 1.134; 3.208	746
15	$CH_2CO \leftrightarrow CH_2C + O$	C−O	−1.66	0.33	1.408; 1.790; 3.818	562
16	$CH_2CO \leftrightarrow CH_2 + CO$	C−C	−0.73	1.31	1.472; 1.839; 2.780	247
17	$CH_2CH \leftrightarrow CHCH + H$	γ-C−H	−1.82	0.38	1.091; 1.118; 3.178	526
18	$CH_2C \leftrightarrow CHC + H$	γ-C−H	−1.26	0.08	1.187; 1.346; 2.292	788
19	$CHC \leftrightarrow CC + H$	γ-C−H	0.08	1.00	1.097; 1,419; 2.956	924
			Bond-Making			
20	$CH_3C \leftrightarrow CH_2CH$	H transfer	+0.20	1.47	1.102; 1.314; 1.165	527
21	$CH_2C + H \leftrightarrow CH_2CH$	C−H	−0.04	0.20	2.739; 1.598; 1.162	687
22	$CH_2CH + H \leftrightarrow C_2H_4$	C−H	−0.02	0.62	2.402; 1.407; 1.096	399
23	$C + O \leftrightarrow CO$	C−O	+1.02	1.99	2.991; 1.750; 1.279	448
24	$H + H \leftrightarrow H_2$	H−H	+1.15	1.18	3.157; 1.107; 0.908	173

CHC species. Third, with more and more hydrogen atoms being stripped off from the C−C backbone of highly dehydrogenated C_2 hydrocarbon species, the C−C bond breaking actually becomes more difficult. Our calculation shows that the activation barrier of the last dehydrogenation step of CHC→CH + C is as high as 2.0 eV. This is also consistent with the strong binding of CHC species with a binding energy of −6.64 eV. As a result, the Mo(110) surface will be coked by the connecting C−C species. The lack of hydrogenation ability of the clean Mo(110) surface results in the total fragmentation of acetaldehyde instead of selective deoxygenation to ethylene. On other transition metal surfaces, the relatively facile C−C bond scission over the C−O bond scission of acetaldehyde will not lead to the desired deoxygenation and will end up with the decarbonylation of acetaldehyde. The C−O cleavage on Mo and C−H bond making on the early transition metals such as Ni and Co could be why CoMo and CoNi are selective for HDO and have been widely used as industrial HDO catalysts.

4. CONCLUSIONS

Acetaldehyde is one of the simplest molecular forms of oxygenates with both C−C and C−O bonds. Acetaldehyde decomposition on the Mo(110) surface serves as a good prototypical reaction to explore the deoxygenation probability of the Mo-based catalyst. Combining density functional theory calculations with the dimer saddle point searching method, a complete decomposition reaction network that consists of several competing reaction pathways via either the C−O or the C−H bond scission of acetaldehyde and reaction intermediates was identified. Compared to the facile C−O or the C−H bond scissions, the C−C bond breaking is kinetically unlikely. This indicates that Mo is capable of acetaldehyde deoxygenation despite strong affinities of Mo toward carbon and oxygen atoms. In general, the C−O bond cleavage is slightly favorable over the C−H bond cleavage because of the strong Mo−O bond. Our calculation results show the selective deoxygenation of acetaldehyde to ethylene is kinetically inhibited by the weak hydrogenation capability of the Mo(110) surface. The vinyl species is easily dehydrogenated into vinylidene and ethynyl instead of being hydrogenated to ethylene. As a result, the nonselective route leading to the accumulations of surface oxygen and ethynyl is the dominant reaction path in acetaldehyde decomposition on the clean Mo(110) surface.

AUTHOR INFORMATION

Corresponding Author

*E-mail: donghai.mei@pnl.gov.

Funding

This work was financially supported by the National Advanced Biofuels Consortium (NABC). Computing time was granted by a user project (emsl42292) at the Molecular Science Computing Facility in the William R. Wiley Environmental Molecular Sciences Laboratory (EMSL). The EMSL is a U.S. Department of Energy (DOE) national scientific user facility located at Pacific Northwest National Laboratory (PNNL) and supported by the DOE Office of Biological and Environmental Research. Pacific Northwest National Laboratory is operated by Battelle for the U.S. Department of Energy.

Notes

The authors declare no competing financial interest.

REFERENCES

(1) Elliott, D. C. *Energy Fuels* **2007**, *21*, 1792.
(2) Huber, G. W.; Iborra, S.; Corma, A. *Chem. Rev.* **2006**, *106*, 4044.

(3) Zakzeski, J.; Bruijnincx, P. C. A.; Jongerius, A. L.; Weckhuysen, B. M. *Chem. Rev.* **2010**, *110*, 3552.
(4) Elliott, D. C.; Beckman, D.; Bridgwater, A. V.; Diebold, J. P.; Gevert, S. B.; Solantausta, Y. *Energy Fuels* **1991**, *5*, 399.
(5) Hong, D. Y.; Miller, S. J.; Agrawal, P. K.; Jones, C. W. *Chem. Commun.* **2010**, *46*, 1038.
(6) Zhao, C.; He, J.; Lemonidou, A. A.; Li, X.; Lercher, J. A. *J. Catal.* **2011**, *280*, 8.
(7) Zhao, C.; Kou, Y.; Lemonidou, A. A.; Li, X. B.; Lercher, J. A. *Angew. Chem., Int. Ed.* **2009**, *48*, 3987.
(8) Zhao, C.; Kou, Y.; Lemonidou, A. A.; Li, X. B.; Lercher, J. A. *Chem. Commun.* **2010**, *46*, 412.
(9) Adanez, J.; de Diego, L. F.; Garcia-Labiano, F.; Gayan, P.; Abad, A.; Palacios, J. M. *Energy Fuels* **2004**, *18*, 371.
(10) Chen, D. A.; Friend, C. M. *J. Am. Chem. Soc.* **1998**, *120*, 5017.
(11) Chen, D. A.; Friend, C. M. *J. Phys. Chem.* **1996**, *100*, 17640.
(12) Chen, D. A.; Friend, C. M. *J. Phys. Chem. B* **1997**, *101*, 5712.
(13) Chen, D. A.; Friend, C. M. *Langmuir* **1998**, *14*, 1451.
(14) Friend, C. M.; Xu, X. *Annu. Rev. Phys. Chem.* **1991**, *42*, 251.
(15) Queeney, K. T.; Friend, C. M. *J. Chem. Phys.* **1998**, *109*, 6067.
(16) Queeney, K. T.; Friend, C. M. *J. Phys. Chem. B* **1998**, *102*, 5178.
(17) Serafin, J. G.; Friend, C. M. *J. Am. Chem. Soc.* **1989**, *111*, 6019.
(18) Serafin, J. G.; Friend, C. M. *J. Am. Chem. Soc.* **1989**, *111*, 4233.
(19) Serafin, J. G.; Friend, C. M. *Surf. Sci.* **1989**, *209*, L163.
(20) Wiegand, B. C.; Uvdal, P.; Serafin, J. G.; Friend, C. M. *J. Phys. Chem.* **1992**, *96*, 5063.
(21) Queeney, K. T.; Arumainayagam, C. R.; Weldon, M. K.; Friend, C. M.; Blumberg, M. Q. *J. Am. Chem. Soc.* **1996**, *118*, 3896.
(22) Zhao, H. B.; Kim, J.; Koel, B. E. *Surf. Sci.* **2003**, *538*, 147.
(23) Davis, J. L.; Barteau, M. A. *J. Am. Chem. Soc.* **1989**, *111*, 1782.
(24) Shekhar, R.; Barteau, M. A.; Plank, R. V.; Vohs, J. M. *J. Phys. Chem. B* **1997**, *101*, 7939.
(25) Norskov, J. K.; Abild-Pedersen, F.; Studt, F.; Bligaard, T. *Proc. Natl. Acad. Sci. U.S.A.* **2011**, *108*, 937.
(26) Alcala, R.; Mavrikakis, M.; Dumesic, J. A. *J. Catal.* **2003**, *218*, 178.
(27) Delbecq, F.; Sautet, P. *Surf. Sci.* **1993**, *295*, 353.
(28) Delbecq, F.; Vigne, F. *J. Phys. Chem. B* **2005**, *109*, 10797.
(29) Mei, D. H.; Karim, A. M.; Wang, Y. *J. Phys. Chem. C* **2011**, *115*, 8155.
(30) Henkelman, G.; Jonsson, H. *J. Chem. Phys.* **1999**, *111*, 7010.
(31) Kresse, G.; Furthmuller, J. *Phys. Rev. B* **1996**, *54*, 11169.
(32) Kresse, G.; Furthmuller, J. *Comput. Mater. Sci.* **1996**, *6*, 15.
(33) Kresse, G.; Hafner, J. *Phys. Rev. B* **1994**, *49*, 14251.
(34) Blochl, P. E.; Jepsen, O.; Andersen, O. K. *Phys. Rev. B* **1994**, *49*, 16223.
(35) Kresse, G.; Joubert, D. *Phys. Rev. B* **1999**, *59*, 1758.
(36) Perdew, J. P.; Chevary, J. A.; Vosko, S. H.; Jackson, K. A.; Pederson, M. R.; Singh, D. J.; Fiolhais, C. *Phys. Rev. B* **1992**, *46*, 6671.
(37) Aghemenloh, E.; Umukoro, J. O.; Azi, S. O.; Yusuf, S.; Idiodi, J. O. A. *Comput. Mater. Sci.* **2011**, *50*, 3290.
(38) Mattheiss, L. F.; Hamann, D. R. *Phys. Rev. B* **1986**, *33*, 823.
(39) Xu, L. J.; Mei, D. H.; Henkelman, G. *J. Chem. Phys.* **2009**, 131.
(40) Mei, D. H.; Xu, L. J.; Henkelman, G. *J. Phys. Chem. C* **2009**, *113*, 4522.
(41) Mei, D. H.; Xu, L.; Henkelman, G. *J. Catal.* **2008**, *258*, 44.
(42) Zhao, Y.-F.; Yang, Y.; Mims, C.; Peden, C. H. F.; Li, J.; Mei, D. *J. Catal.* **2011**, *281*, 199.
(43) Mavrikakis, M.; Barteau, M. A. *J. Mol. Catal. A: Chem.* **1998**, *131*, 135.
(44) Houtman, C. J.; Barteau, M. A. *J. Catal.* **1991**, *130*, 528.
(45) McCabe, R. W.; Dimaggio, C. L.; Madix, R. J. *J. Phys. Chem.* **1985**, *89*, 854.
(46) Jeroro, E.; Vohs, J. M. *J. Phys. Chem. C* **2009**, *113*, 1486.
(47) Fruhberger, B.; Chen, J. G. *J. Am. Chem. Soc.* **1996**, *118*, 11599.
(48) Fernandez, E. M.; Moses, P. G.; Toftelund, A.; Hansen, H. A.; Martinez, J. I.; Abild-Pedersen, F.; Kleis, J.; Hinnemann, B.; Rossmeisl, J.; Bligaard, T.; Norskov, J. K. *Angew. Chem., Int. Ed.* **2008**, *47*, 4683.
(49) Vojvodic, A.; Calle-Vallejo, F.; Guo, W.; Wang, S.; Toftelund, A.; Studt, F.; Martinez, J. I.; Shen, J.; Man, I. C.; Rossmeisl, J.; Bligaard, T.; Norskov, J. K.; Abild-Pedersen, F. *J. Chem. Phys.* **2011**, 134.
(50) Norskov, J. K.; Bligaard, T.; Logadottir, A.; Bahn, S.; Hansen, L. B.; Bollinger, M.; Bengaard, H.; Hammer, B.; Sljivancanin, Z.; Mavrikakis, M.; Xu, Y.; Dahl, S.; Jacobsen, C. J. H. *J. Catal.* **2002**, *209*, 275.
(51) Liu, B.; Greeley, J. *J. Phys. Chem. C* **2011**, *115*, 19702.
(52) Ferrin, P.; Simonetti, D.; Kandoi, S.; Kunkes, E.; Dumesic, J. A.; Nørskov, J. K.; Mavrikakis, M. *J. Am. Chem. Soc.* **2009**, *131*, 5809.
(53) Loffreda, D.; Delbecq, F.; Vigne, F.; Sautet, P. *Angew. Chem., Int. Ed.* **2009**, *48*, 8978.
(54) Gu, X.-K.; Li, W.-X. *J. Phys. Chem. C* **2010**, *114*, 21539.